Original Article

Aneurysmal wall enhancement and hemodynamics: pixel-level correlation between spatial distribution

Mingzhu Fu[1#], Fei Peng[2,3,4#], Miaoqi Zhang[1], Shuo Chen[1], Hao Niu[2,3,4], Xiaoxin He[2,3,4], Boya Xu[2,3,4], Aihua Liu[2,3,4], Rui Li[1]

[1]Center for Biomedical Imaging Research, Department of Biomedical Engineering, School of Medicine, Tsinghua University, Beijing, China; [2]Beijing Neurosurgical Institute, Capital Medical University, Beijing, China; [3]Department of Interventional Neuroradiology, Beijing Tiantan Hospital, Beijing, China; [4]China National Clinical Research Center for Neurological Diseases, Beijing, China

Contributions: (I) Conception and design: M Fu, F Peng; (II) Administrative support: A Liu, R Li; (III) Provision of study materials or patients: All authors; (IV) Collection and assembly of data: All authors; (V) Data analysis and interpretation: All authors; (VI) Manuscript writing: All authors; (VII) Final approval of manuscript: All authors.

[#]These authors contributed equally to this work.

Correspondence to: Aihua Liu. Beijing Neurosurgical Institute, Capital Medical University; Department of Interventional Neuroradiology, Beijing Tiantan Hospital, Capital Medical University; China National Clinical Research Center for Neurological Diseases, 119 South 4th Ring West Road, Fengtai District, Beijing 100070, China. Email: liuaihuadoctor@163.com; Rui Li. Center for Biomedical Imaging Research, Department of Biomedical Engineering, School of Medicine, Tsinghua University, Beijing 100084, China. Email: leerui@tsinghua.edu.cn.

Background: Inflammation and hemodynamics are interrelated risk factors for intracranial aneurysm rupture. This study aimed to identify the relationship between these risk factors from an individual-patient perspective using biomarkers of aneurysm wall enhancement (AWE) derived from high-resolution magnetic resonance imaging (HR-MRI) and hemodynamic parameters by four-dimensional flow MRI (4D-flow MRI).

Methods: A total of 29 patients with 29 unruptured intracranial aneurysms larger than 4 mm were included in this prospective cross-sectional study. A total of 24 aneurysms had AWE and 5 did not have AWE. A three-dimensional (3D) vessel model of each individual aneurysm was generated with 3D time-of-flight magnetic resonance angiography (3D TOF-MRA). Quantification of AWE was sampled with HR-MRI. Time-averaged wall shear stress (WSS) and oscillatory shear index (OSI) were calculated from the 4D-flow MRI. The correlation between spatial distribution of AWE and hemodynamic parameters measured at pixel-level was evaluated for each aneurysm.

Results: In aneurysms with AWE, the spatial distribution of WSS was negatively correlated with AWE in 100% (24/24) of aneurysms, though 2 had an absolute value of the correlation coefficient <0.1. The OSI was positively correlated with AWE in 91.7% (22/24) of aneurysms; the other 2 aneurysms showed a negative correlation with AWE. In aneurysms with no AWE, there was no correlation between WSS (100%, 5/5), OSI (80%, 4/5), and wall inflammation.

Conclusions: The spatial distribution of WSS was negatively correlated with AWE in aneurysms with AWE, and OSI was positively correlated with AWE in most aneurysms with AWE. While aneurysms that did not contain AWE showed no correlation between hemodynamics and wall inflammation.

Keywords: Unruptured intracranial aneurysms (UIAs); hemodynamics; aneurysmal wall enhancement; individual-patient

Submitted Dec 12, 2021. Accepted for publication Mar 29, 2022.
doi: 10.21037/qims-21-1203
View this article at: https://dx.doi.org/10.21037/qims-21-1203

© Quantitative Imaging in Medicine and Surgery. All rights reserved.

Introduction

Unruptured intracranial aneurysms (UIAs) are local dilatations on the wall of intracranial arteries. The prevalence of UIAs is 3–7% in the adult population worldwide (1,2). In a study including 11,660 aneurysm-years, the annual rupture risk was reported to be 0.95% (3). Once ruptured, UIAs can cause intracranial subarachnoid hemorrhage, which has a mortality rate of up to 50% (4). Histopathological evidence from human and animal studies has suggested that the inflammatory processes in the aneurysmal wall may play a role in the formation, growth, and rupture of the aneurysm (5,6). Aneurysm wall enhancement (AWE) on high-resolution magnetic resonance imaging (HR-MRI) has been used as an indicator of wall inflammation and weakening of the aneurysm wall (7,8). Recent studies have found that several factors could contribute to AWE except wall inflammation, particularly low-flow patterns, which could lead to pseudo-enhancement of the aneurysm wall (9,10). In 2 other phantom studies, it was demonstrated that near-wall slow flow mimicked wall enhancement in HR-MRI (11,12). These findings did not refute the clinical value of HR-MRI, but hinted that studies of AWE should be carefully conducted, with measures taken to reduce the impact of low-flow patterns.

Previous studies have hypothesized a pathogenetic link between hemodynamics and inflammatory vessel wall alteration leading to the development and rupture of UIAs, and many studies have explored this association (13-16). Based on computational fluid dynamics (CFD) and HR-MRI, several studies found that AWE regions were associated with lower wall shear stress (WSS), which is the most highlighted hemodynamic parameter, and WSS was found to be an independent predictor of AWE (17-19). With the same methods, another study showed that the association between AWE and hemodynamics seemed to depend on the location of the AWE region (20). One study used four-dimensional flow MRI (4D-flow MRI), which allows direct *in vivo* and reliable hemodynamic measurement of UIAs (21,22), to explore the relationship between hemodynamics and AWE and also found that low WSS was independently associated with high AWE grade (23). However, all of these studies compared groups of aneurysms; they did not reflect the spatial distribution correlation between aneurysmal wall inflammation and hemodynamics at the individual-patient level.

In this study, taking advantage of HR-MRI and 4D-flow MRI, the relationship between distribution of AWE and hemodynamic parameters on aneurysmal wall was studied from a pixel-level perspective for each specific patient. We aimed to provide new insights into the relationship between hemodynamics and inflammation processes in UIAs. We present the following article in accordance with the STROBE reporting checklist (available at https://qims.amegroups.com/article/view/10.21037/qims-21-1203/rc).

Methods

Study population

This prospective cross-sectional study was approved by the local Institutional Ethics Committee of Tsinghua University and Beijing Tiantan Hospital, and all participants provided written informed consent. Patients with UIAs detected by digital subtraction angiography (DSA), computed tomographic angiography (CTA), or magnetic resonance angiography (MRA) were recruited from Beijing Tiantan Hospital between 2014 to 2017. The inclusion criteria were as follows: (I) patients with no contraindications to MRI; and (II) patients with aneurysms larger than 4 mm. The exclusion criteria were as follows: (I) patients with poor image quality; (II) patients who had a history of surgical clipping or endovascular treatment; and (III) patients with fusiform, dissecting, and thrombosed aneurysms. The study was conducted in accordance with the Declaration of Helsinki (as revised in 2013).

MRI protocol

All MRI scans were conducted on a 3.0T MR scanner (Achieva TX, Philips, Best, The Netherlands) with a 32-channel head coil. First, the 3D time-of-flight MRA (3D TOF-MRA) was acquired, and the aneurysm was located. The imaging parameters for 3D TOF-MRA were as follows: repetition time/echo time (TR/TE) =25/3.5 ms, field of view (FOV) =160×160×60 mm^3, voxel size =0.8×0.8×0.8 mm^3, and flip angle =20°. Then, 4D-flow MRI was acquired using a free-breathing, peripheral pulse-gated, multi-shot turbo filed echo sequence, and the scan parameters were as follows: TR/TE =8.0/3.6 ms, FOV =160×160×30 mm^3, voxel size =1×1×1 mm^3, flip angle =20°, and velocity encoding (VENC) =120 cm/s for all 3 directions. Furthermore, pre- and post-contrast HR-MRI were performed using a 3D black-blood T1-weighted volumetric isotropic turbo spin echo acquisition (3D T1-VISTA) sequence with a variable flip angle (24),

© Quantitative Imaging in Medicine and Surgery. All rights reserved.

and the other imaging parameters were as follows: TR/TE =800/21 ms, FOV =200×180×40 mm^3, and voxel size =0.6×0.6×0.6 mm^3. Post-contrast HR-MRI was imaged after the intravenous injection of gadolinium diethylenetriamine penta-acetic acid (GdDTPA; Magnevist; Bayer Schering Pharma, Berlin, Germany) for about 6 minutes at a dose of 0.1 mmol/kg.

AWE analysis

Based on the pre- and post-contrast HR-MRI images, the existence of AWE was determined by 2 experienced neuroradiologists (with >4 years' experience in neurovascular imaging) who were blinded to the patients' clinical data and other sequences except for 3D TOF-MRA. Any disagreement between the 2 readers was resolved by consensus. An aneurysm with AWE was defined when part or whole of the aneurysmal wall was enhanced, while an aneurysm with no AWE was defined when there was no enhanced area on the aneurysmal wall.

The maximum height from the aneurysm neck to the dome tip was defined as the UIAs size and measured with pre-contrast HR-MRI (25). To explore the relationship between the spatial distribution of AWE and hemodynamic parameters on the aneurysmal wall, an image postprocessing workflow utilizing multi-contrast images was proposed (*Figure 1*). First, regarding the large amount of 4D-flow MRI data and reserving the speed information, 3D TOF-MRA and post-contrast HR-MRI were registered to 4D-flow MRI using an automatic volumetric rigid registration method (i.e., *elastix*) in 3D Slicer (www.slicer.org). Then, to quantify the AWE spatial distribution in consideration of eliminating the pseudo-enhancement induced by near-wall slow flow, a method similar to that described by Khan *et al.*, (19) and Raghuram *et al.*, (26) was used. Explicitly, the 3D vessel model was generated from the registered 3D TOF-MRA based on algorithms, including threshold segmentation, region growth, connected domain selection, and surface smoothing in our custom-built software programmed in Python. Next, the image signal intensity of post-contrast HR-MRI was projected onto the 3D vessel model and then averaged along the length of the line that was normal to each mesh node. In doing so, the AWE distribution could be objectively analyzed and used to better observe the distribution along the aneurysm wall in 3D space. The sampling and projecting processes were also performed for aneurysms with no AWE to show their wall situation.

Hemodynamic analysis

Preprocessing steps of 4D-flow MRI, including eddy current correction and velocity mask application, were performed to ensure the vessel had accurate velocity results. The distribution of the velocity arrows was plotted to observe and show the blood flow inside the aneurysm. We then calculated the hemodynamic parameters of WSS and oscillatory shear index (OSI). The WSS is the frictional force of the flowing blood on the vessel wall and is defined as the velocity gradient along the inward perpendicular path of the vessel wall. Here, the estimation of WSS was performed based on a validated quantitative analysis method at all timepoints during a cardiac cycle (27). Then, the time-averaged WSS, named aWSS, was calculated using the obtained WSS at all timepoints with the following formula:

$$aWSS = \frac{1}{T}\int_0^\tau \left|\overrightarrow{WSS_t}\right| dt \quad [1]$$

Where $\overrightarrow{WSS_t}$ was instantaneous WSS vectors. After that, the OSI, denoting the fluctuation of WSS (28), was calculated with the following formula:

$$OSI = \frac{1}{2}\left(1 - \frac{\left|\int_0^\tau \overrightarrow{wss_t} dt\right|}{\int_0^\tau \left|\overrightarrow{wss_t}\right| dt}\right) \quad [2]$$

After the spatial distribution quantification of AWE and hemodynamic parameters, the interfering blood vessels around the aneurysm in the 3D model were clipped. Then, the spatial distribution of AWE and hemodynamic parameters was highlighted and obtained with a region of interest (ROI)-selecting box, as shown in *Figure 1*.

Statistical analysis

Statistical analysis was conducted using Python packages Scipy and Stats models (https://pypi.org). Data were expressed as count (percentage) or median (interquartile range). The agreement between 2 observers for the existence of AWE was evaluated by a κ value and the interobserver reliability evaluation for the continuous variables was using Bland-Altman plots. To study the distribution characteristics of hemodynamics on different enhanced areas, the aneurysm was divided into a low-enhanced area and high-enhanced area using its median of image signal intensities as a threshold. Their corresponding hemodynamic parameters were also analyzed with the Mann-Whitney U test. Furthermore, Spearman's correlation analysis was used to investigate the association

© Quantitative Imaging in Medicine and Surgery. All rights reserved.

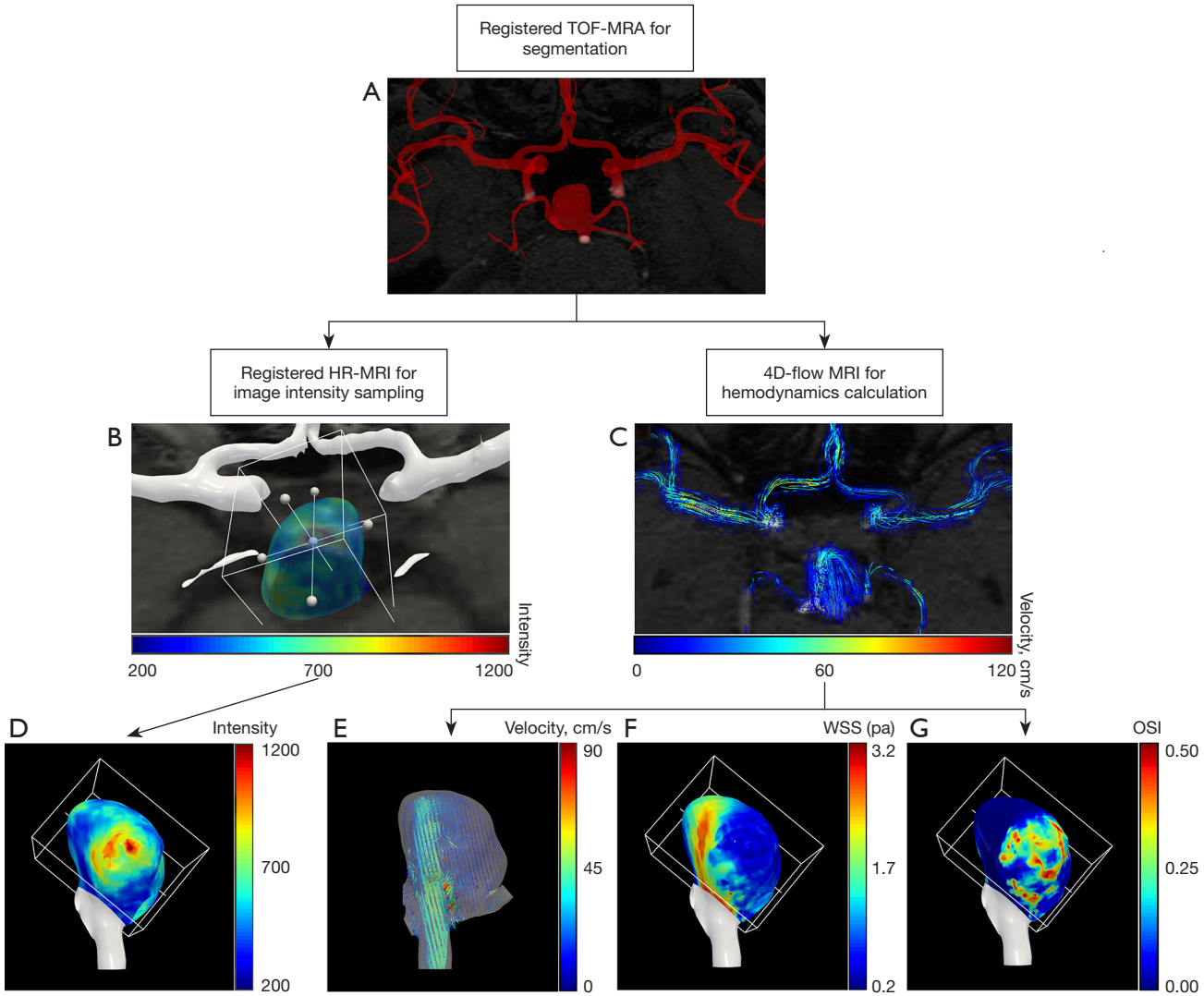

Figure 1 Image processing workflow. (A) The 3D vessel model including aneurysm was generated with the registered 3D magnetic resonance angiography (TOF-MRA). (B) The registered post-contrast HR-MRI was used to be sampled by the 3D vessel model and obtain the spatial distribution of image intensity indicating AWE. (C) Three-dimensional velocity filed calculated from 4D-flow MRI was used for calculation of hemodynamic parameters including WSS and OSI. (E) Velocity distribution inside the aneurysm was used to observe the blood flow near the aneurysm wall. (D,F,G) The spatial distribution of image intensity indicating AWE (D), WSS (F), and OSI (G) was highlighted and obtained by the same ROI-selecting box. TOF-MRA, time-of-flight magnetic resonance angiography; HR-MRI, high-resolution magnetic resonance imaging; AWE, aneurysmal wall enhancement; MRI, magnetic resonance imaging; WSS, wall shear stress; OSI, oscillatory shear index; ROI, region of interest.

between spatial distribution of AWE and hemodynamic parameters on aneurysmal wall. A P value <0.05 was considered statistically significant.

Results

A total of 17 patients were excluded: 5 with poor image quality, 3 with aneurysms smaller than 4 mm, and 9 with fusiform, dissecting, or thrombosed aneurysms (*Figure 2*). Finally, a total of 29 patients with 29 UIAs were recruited in the study, of which 24 aneurysms showed AWE and 5 aneurysms showed no AWE. The 2 readers' discrimination for AWE existence was well-matched (κ=0.86). The clinical characteristics of participants are summarized in *Table 1*.

© Quantitative Imaging in Medicine and Surgery. All rights reserved.

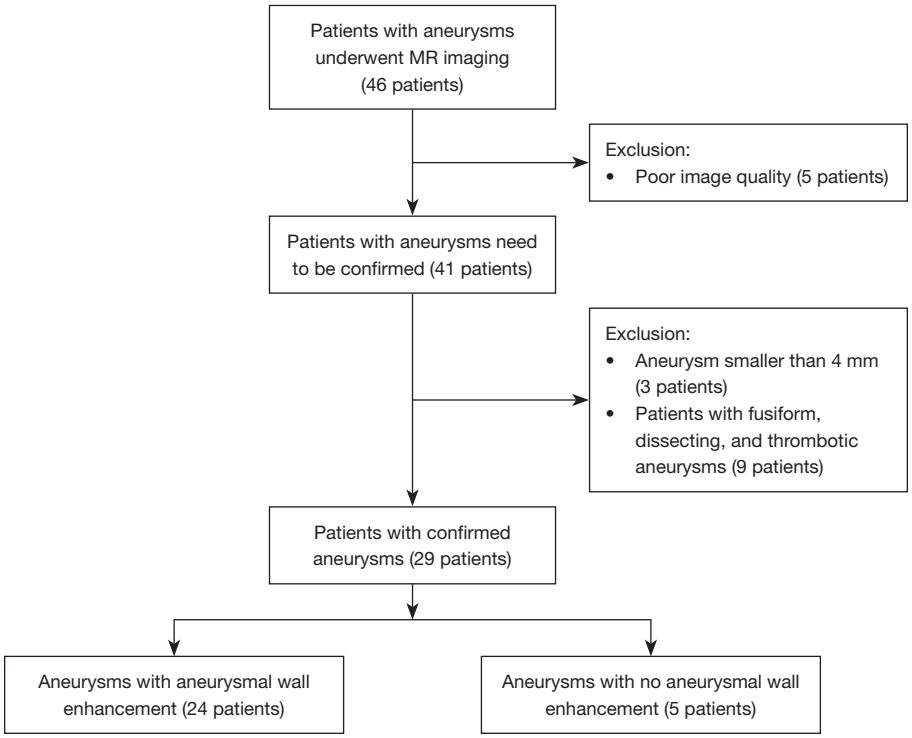

Figure 2 Flowchart of patients' selection.

Table 1 Patient characteristics of the study population (n=29)

Parameter	AWE (n=24)	No AWE (n=5)
Mean age ≥50 years	20 (69.0%)	5 (17.2%)
Gender		
Female	16 (55.2%)	3 (10.3%)
Male	8 (27.6%)	2 (6.9%)
Hypertension	12 (41.4%)	3 (10.3%)
Smoking	7 (24.1%)	0 (0%)
Hyperlipidemia	10 (34.5%)	2 (6.9%)
Diabetes	4 (13.8%)	2 (6.9%)
UIA location		
Anterior circulation	12 (41.4%)	0 (0%)
Posterior circulation	12 (41.4%)	5 (17.2%)
UIA Size ≥7 mm	22 (75.9%)	0 (0%)

AWE, aneurysmal wall enhancement; UIA, unruptured intracranial aneurysm.

The interobserver reliability for continuous variable evaluation is shown in *Figure 3*. All parameters measured by MRI showed good reliability. The results revealed that 82.8% (24/29) of aneurysms had AWE and 17.2% (5/29) of aneurysms did not have AWE. Among the aneurysms with AWE, 91.7% (22/24) had significantly lower WSS and higher OSI in the high enhanced area compared to the low enhanced area. Among the aneurysms without AWE, 100% (5/5) had no significant difference between WSS in the different areas and 80% (4/5) of them had no significant difference between OSI in the different areas. The detailed comparison results of the low-enhanced area and high-enhanced area for each aneurysm are shown in *Table 2*.

To further identify the relationship between the spatial distribution of AWE and hemodynamic parameters, Spearman's correlation analysis was conducted for each aneurysm (*Table 3*). The results showed that WSS was negatively correlated with AWE in 100% (24/24) of aneurysms with AWE, although 2 cases had an absolute

© Quantitative Imaging in Medicine and Surgery. All rights reserved.

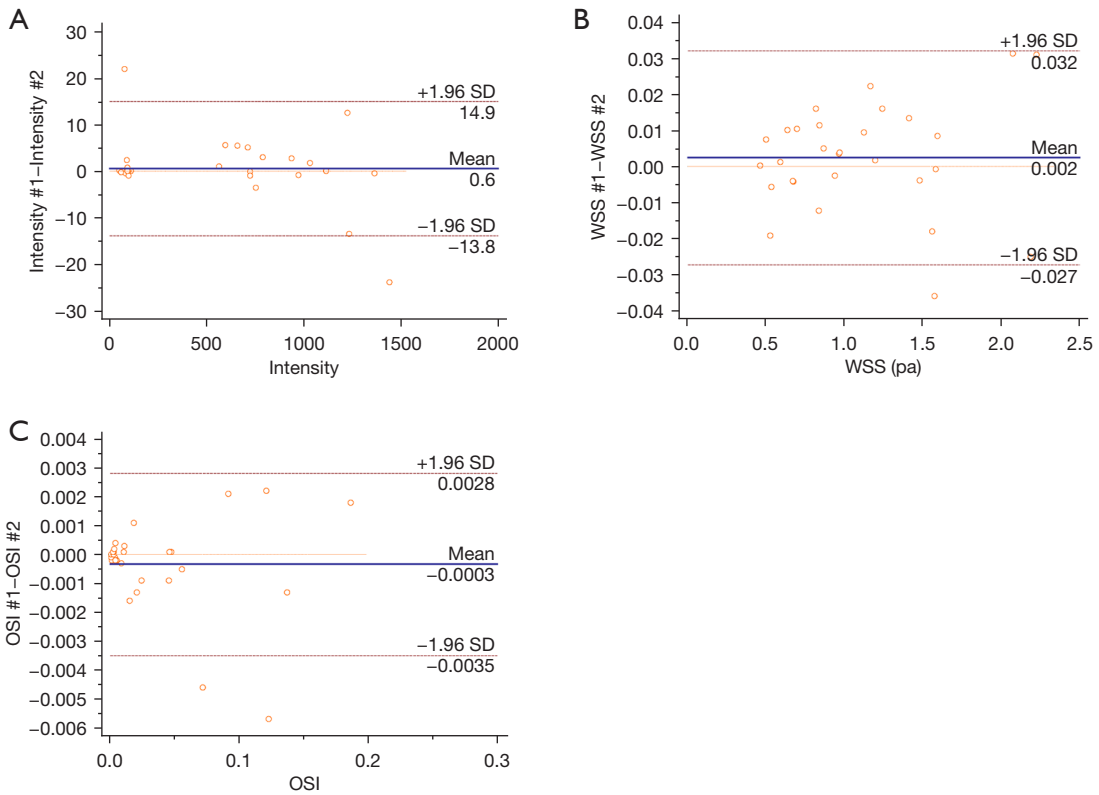

Figure 3 Bland-Altman plots for the interobserver reliability evaluation of continuous variables. (A) Image intensity indicating AWE. (B) WSS. (C) OSI. AWE, aneurysmal wall enhancement; WSS, wall shear stress; OSI, oscillatory shear stress.

value of the correlation coefficient smaller than 0.1. Meanwhile, OSI was found to be positively correlated with AWE in 91.7% (22/24) of aneurysms with AWE, while the other 2 cases showed a negative correlation. However, in aneurysms with no AWE, there was no correlation between WSS (100%, 5/5), OSI (80%, 4/5), and signal intensities that indicated wall inflammation.

Figure 4 shows the spatial distribution of image intensity indicating AWE and hemodynamics in 4 cases of aneurysms, of which 2 had AWE while the other 2 did not. Distribution of velocity arrows inside the aneurysm was also presented for each aneurysm in the figure. The corresponding distribution map of AWE, WSS, and OSI in aneurysms with AWE clearly showed that the part of the aneurysm with higher AWE (indicated by a large arrow) tended to have lower WSS and higher OSI, while the part of the aneurysm with lower AWE (indicated by a small arrow) tended to have higher WSS and lower OSI. However, the corresponding distribution map in aneurysms with no AWE showed no obvious distribution characteristics. Velocity arrows plotted in the figure represented the qualitatively associated distribution of velocity near aneurysm wall with WSS. Scatter plots and regression lines were also created to show the relationship between the spatial distribution of image intensity indicating AWE and hemodynamic parameters for these 4 aneurysms (*Figure 5*). The results also showed that WSS was negatively correlated with AWE and OSI was positively correlated with AWE in aneurysms with AWE. And in aneurysms with no AWE, there were no correlations between them.

Discussion

The rapid development of new MRI technologies, including 4D-flow MRI and HR-MRI, has made it possible to visualize and evaluate AWE and hemodynamic characteristics in recent years (29,30). In this study, 4D-flow MRI and HR-MRI were used to investigate the relationship between distribution of AWE and hemodynamic parameters on UIAs. Our findings support the notion that low WSS

© Quantitative Imaging in Medicine and Surgery. All rights reserved.

Table 2 Comparison results of hemodynamics between the low-enhanced area and high-enhanced area for 29 aneurysms, individually

	Patient	Size (mm)	WSS (pa)			OSI		
			Low-enhanced	High-enhanced	P value	Low-enhanced	High-enhanced	P value
AWE	# 01	9.7	1.0664 (0.7673, 1.5167)	0.9184 (0.6106, 1.3492)	<0.001*	0.0086 (0.0031, 0.0216)	0.0093 (0.0037, 0.0361)	0.012
	# 02	12.6	0.9691 (0.7033, 1.4426)	0.8596 (0.5868, 1.1959)	<0.001*	0.0192 (0.0044, 0.0917)	0.0376 (0.0105, 0.1150)	<0.001*
	# 03	10.4	2.2168 (1.8418, 2.6341)	1.9030 (1.5741, 2.2051)	<0.001*	0.0029 (0.0016, 0.0075)	0.0045 (0.0022, 0.0120)	<0.001*
	# 04	9.9	1.7490 (1.3400, 2.3000	1.5916 (1.2751, 1.7986)	<0.001*	0.0022 (0.0011, 0.0062)	0.0040 (0.0022, 0.0078)	<0.001*
	# 05	11.2	1.8554 (1.3947, 2.5090)	1.4727 (1.0368, 1.8517)	<0.001*	0.0028 (0.001, 0.0081)	0.0054 (0.0018, 0.018)	<0.001*
	# 06	9.8	1.1937 (0.9985, 1.5100)	1.1351 (0.8419, 1.4718)	<0.001*	0.0082 (0.0036, 0.0196)	0.0108 (0.004, 0.0296)	<0.001*
	# 07	17.8	0.8540 (0.6327, 1.3543)	0.7087 (0.5668, 0.9418)	<0.001*	0.0246 (0.0039, 0.1592)	0.2015 (0.0470, 0.2956)	<0.001*
	# 08	11.9	1.6127 (1.3511, 1.7805)	1.5822 (1.3678, 1.7148)	0.002	0.0022 (0.0012, 0.0058)	0.0017 (0.0008, 0.0048)	<0.001*
	# 09	8.2	2.4710 (2.002, 2.9528)	1.6148 (1.2368, 2.2834)	<0.001*	0.0008 (0.0003, 0.0018)	0.0030 (0.0012, 0.0124)	<0.001*
	# 10	6.6	2.2356 (1.8736, 2.5832)	2.1704 (1.6964, 2.5099)	<0.001*	0.0013 (0.0006, 0.0028)	0.0019 (0.0008, 0.0062)	<0.001*
	# 11	8.0	1.5890 (0.9397, 3.1208)	1.3651 (0.8528, 2.1204)	<0.001*	0.0024 (0.0006, 0.0085)	0.0041 (0.0011, 0.0222)	<0.001*
	# 12	12.5	0.8096 (0.3553, 1.7069)	0.6642 (0.3357, 0.9858)	<0.001*	0.0336 (0.0027, 0.1167)	0.0434 (0.0071, 0.1518)	<0.001*
	# 13	18.4	0.6248 (0.4842, 0.8999)	0.6604 (0.5024, 0.8512)	0.197	0.0564 (0.0106, 0.1622)	0.0804 (0.0284, 0.1613)	<0.001*
	# 14	9.6	2.6593 (2.2816, 2.9309)	2.1206 (1.6834, 2.4719)	<0.001*	0.0024 (0.0012, 0.0046)	0.0039 (0.0014, 0.0089)	<0.001*
	# 15	10.9	0.4956 (0.3818, 0.6508)	0.4356 (0.3599, 0.5337)	<0.001*	0.0330 (0.0118, 0.0879)	0.0587 (0.0266, 0.1330)	<0.001*
	# 16	7.1	1.1523 (0.9028, 1.4828)	0.9130 (0.7248, 1.1090)	<0.001*	0.0281 (0.0089, 0.0643)	0.0760 (0.0362, 0.1611)	<0.001*
	# 17	9.8	0.6249 (0.5061, 0.8016)	0.5306 (0.4430, 0.6272)	<0.001*	0.0709 (0.0338, 0.1211)	0.1152 (0.0558, 0.1949)	<0.001*
	# 18	10.4	0.7549 (0.5358, 1.0465)	0.9064 (0.6442, 1.2312)	<0.001*	0.0303 (0.0086, 0.0887)	0.0130 (0.0041, 0.0685)	<0.001*
	# 19	7.54	0.7345 (0.4837, 1.1033)	0.4684 (0.4089, 0.5686)	<0.001*	0.0416 (0.0122, 0.1286)	0.1269 (0.0644, 0.1945)	<0.001*
	# 20	11.7	0.7461 (0.5445, 1.0478)	0.5216 (0.4140, 0.6621)	<0.001*	0.0345 (0.0102, 0.1364)	0.1866 (0.1064, 0.2722)	<0.001*
	# 21	5.2	0.4905 (0.3762, 0.6284)	0.4155 (0.317, 0.5664)	<0.001*	0.0410 (0.0095, 0.0992)	0.0841 (0.0288, 0.1754)	<0.001*
	# 22	8.7	1.5616 (1.2339, 1.7772)	1.2588 (1.0450, 1.4996)	<0.001*	0.0023 (0.0012, 0.0047)	0.0048 (0.0023, 0.0100)	<0.001*
	# 23	8.8	0.8410 (0.7586, 0.9588)	0.7607 (0.6066, 0.8912)	<0.001*	0.0394 (0.0197, 0.0992)	0.0650 (0.0254, 0.1536)	<0.001*
	# 24	9.9	0.8182 (0.6691, 1.0427)	0.5897 (0.4652, 0.7745)	<0.001*	0.0606 (0.0263, 0.1394)	0.1833 (0.0827, 0.2768)	<0.001*
No AWE	# 25	6.2	1.1921 (0.8675, 1.4903)	1.203 (0.9296, 1.3933)	0.221	0.0058 (0.0023, 0.0158)	0.0052 (0.0025, 0.0129)	0.324
	# 26	4.8	1.1912 (0.3822, 2.4922)	0.8928 (0.4436, 2.4146)	0.345	0.0082 (0.0014, 0.0288)	0.0092 (0.0017, 0.0224)	0.433
	# 27	5.6	1.6672 (1.2170, 2.104)	1.6369 (1.2628, 2.1849)	0.491	0.0025 (0.0011, 0.0055)	0.0038 (0.0016, 0.0096)	<0.001*
	# 28	4.3	0.8252 (0.6096, 1.2124)	0.9335 (0.6143, 1.269)	0.220	0.0159 (0.0066, 0.0336)	0.0148 (0.0078, 0.0316)	0.289
	# 29	5.2	1.2398 (1.068, 1.4823)	1.2639 (0.9642, 1.683)	0.208	0.0048 (0.0027, 0.0080)	0.0038 (0.0019, 0.0127)	0.230

*, P<0.001. AWE, aneurysmal wall enhancement; WSS, wall shear stress; OSI, oscillatory shear index.

and high OSI are associated with high AWE on UIAs. To our knowledge, this was the first study to evaluate the 3D spatial distribution of AWE and hemodynamic parameters for UIAs from a pixel-level perspective at the individual-patient level.

In this study, statistical results showed that WSS was significantly lower and OSI was significantly higher in the high-enhanced area than in the low-enhanced area of aneurysms with AWE, while they showed no significant difference in different enhanced areas of aneurysm with

© Quantitative Imaging in Medicine and Surgery. All rights reserved.

Table 3 Spearman's correlation analysis results for 29 aneurysms, individually

	Patient	Size (mm)	WSS (pa)		OSI	
			Correlation coefficient	P value	Correlation coefficient	P value
AWE	# 01	9.7	−0.248	<0.001*	0.211	<0.001*
	# 02	12.6	−0.236	<0.001*	0.254	<0.001*
	# 03	10.4	−0.211	<0.001*	0.202	<0.001*
	# 04	9.9	−0.322	<0.001*	0.301	<0.001*
	# 05	11.2	−0.305	<0.001*	0.240	<0.001*
	# 06	9.8	−0.117	<0.001*	0.116	<0.001*
	# 07	17.8	−0.225	<0.001*	0.392	<0.001*
	# 08	11.9	−0.056	0.046	−0.195	<0.001*
	# 09	8.2	−0.373	<0.001*	0.407	<0.001*
	# 10	6.6	−0.178	<0.001*	0.242	<0.001*
	# 11	8.0	−0.243	<0.001*	0.318	<0.001*
	# 12	12.5	−0.287	<0.001*	0.193	<0.001*
	# 13	18.4	−0.031	<0.001*	0.153	<0.001*
	# 14	9.6	−0.554	<0.001*	0.215	<0.001*
	# 15	10.9	−0.341	<0.001*	0.291	<0.001*
	# 16	7.1	−0.401	<0.001*	0.448	<0.001*
	# 17	9.8	−0.350	<0.001*	0.325	<0.001*
	# 18	10.4	0.246	<0.001*	−0.161	<0.001*
	# 19	7.54	−0.439	<0.001*	0.340	<0.001*
	# 20	11.7	−0.437	<0.001*	0.495	<0.001*
	# 21	5.2	−0.216	<0.001*	0.309	<0.001*
	# 22	8.7	−0.316	<0.001*	0.325	<0.001*
	# 23	8.8	−0.317	<0.001*	0.116	<0.001*
	# 24	9.9	−0.435	<0.001*	0.409	<0.001*
No AWE	# 25	6.2	−0.024	0.453	−0.026	0.415
	# 26	4.8	−0.021	0.676	0.027	0.603
	# 27	5.6	0.023	0.455	0.160	<0.001*
	# 28	4.3	0.046	0.360	0.075	0.137
	# 29	5.2	0.029	0.487	−0.039	0.340

*, P<0.001. AWE, aneurysmal wall enhancement; WSS, wall shear stress; OSI, oscillatory shear index.

no AWE (*Table 2*; *Figure 4*). Furthermore, Spearman's correlation analysis verified the negative correlation between WSS and AWE and a positive correlation between OSI and AWE in aneurysms with AWE and almost no correlation in aneurysms with no AWE (*Table 3*; *Figure 5*). As WSS denotes the tangential force on the aneurysmal wall exerted by the horizontal blood flow and OSI reflects fluctuations and oscillations of WSS (31,32), low WSS and high OSI may reflect a vortex or helical flow, which may induce an inflammatory response of the aneurysmal

© Quantitative Imaging in Medicine and Surgery. All rights reserved.

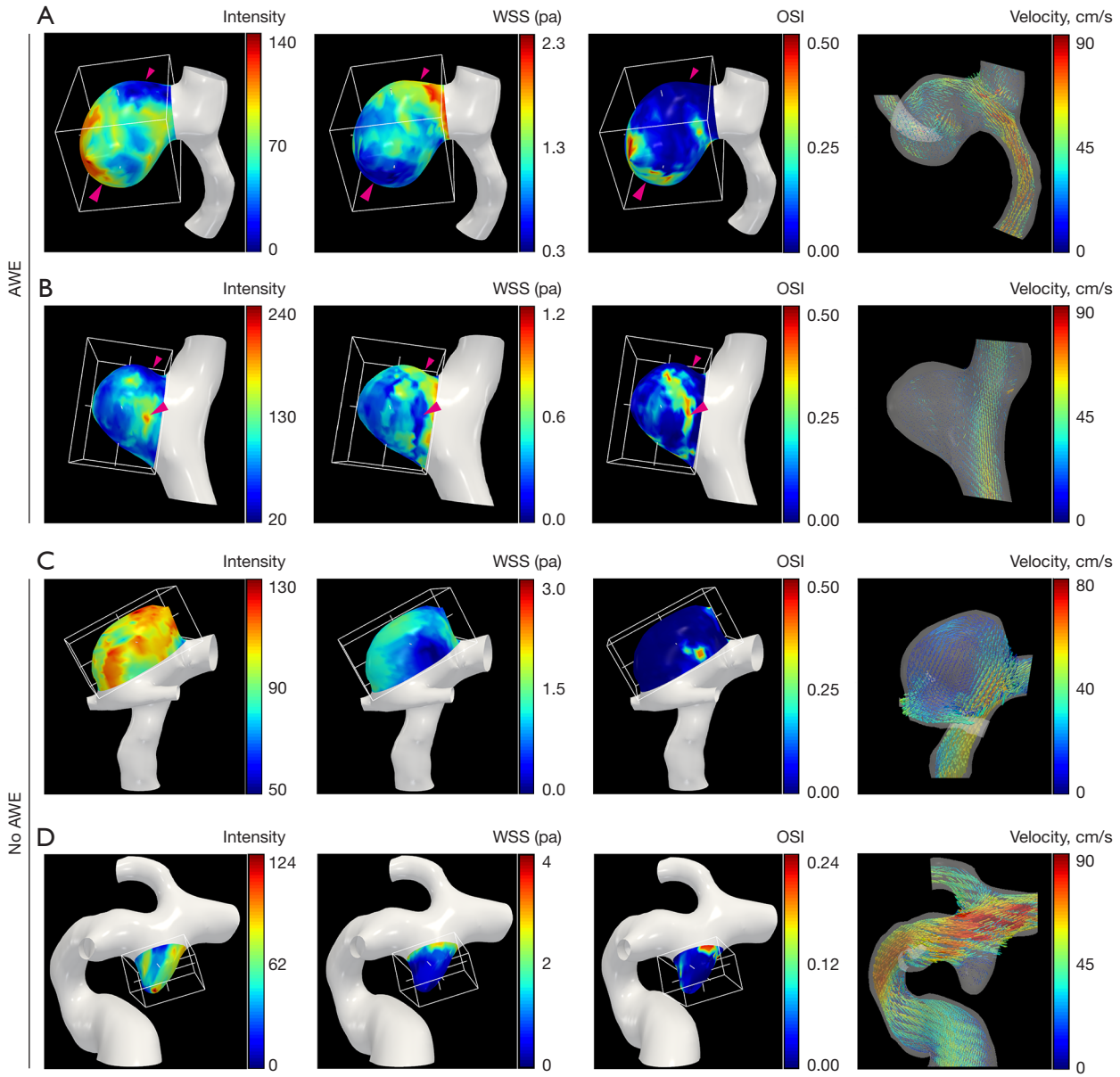

Figure 4 Corresponding distribution map of image intensity indicating AWE, WSS, and OSI for 2 cases of aneurysms with AWE and 2 cases of aneurysms with no AWE. (A) Aneurysm with AWE located at the anterior communicating artery. (B) Aneurysm with AWE located at the basilar artery. The part of aneurysm with higher AWE (large arrow) tended to have lower WSS and higher OSI, while the part of aneurysm with lower AWE (small arrow) tended to have higher WSS and lower OSI. (C) Aneurysm with no AWE located at the anterior communicating artery. (D) Aneurysm with no AWE located at the internal carotid artery. AWE, aneurysmal wall enhancement; WSS, wall shear stress; OSI, oscillatory shear index.

wall and stimulate the progression of atherosclerosis, manifesting as AWE (33). In a rat aneurysm model, low WSS and high OSI were shown to promote macrophage-mediated inflammation of the aneurysmal wall, which is consistent with our results (34). In recent years, the associations between AWE and hemodynamic parameters have been widely investigated among patient populations. Previous studies have concluded that a low WSS was independently associated with AWE, which is in line with our results (17-19). Regarding OSI, a study by Xiao *et al.* (17)

© Quantitative Imaging in Medicine and Surgery. All rights reserved.

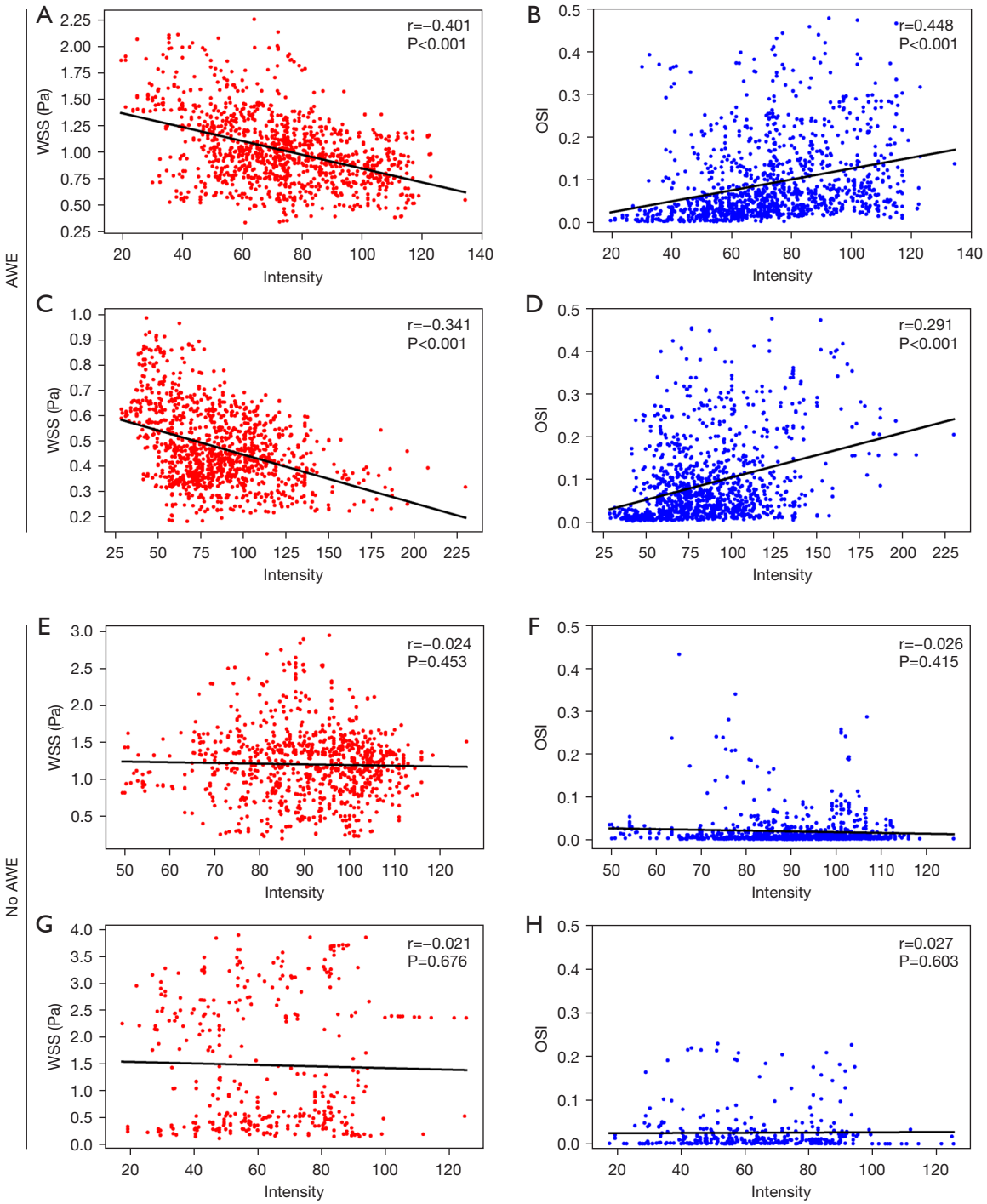

Figure 5 Scatter plots of image intensity indicating AWE and hemodynamic parameters for all pixels from each one of the four aneurysm cases. (A,B) Scatter plots for the aneurysm with AWE located at the anterior communicating artery. (C,D) Scatter plots for the aneurysm with AWE located at the basilar artery. (E,F) Scatter plots for the aneurysm with no AWE located at the anterior communicating artery. (G,H) Scatter plots for the aneurysm with no AWE located at the internal carotid artery. AWE, aneurysmal wall enhancement; WSS, wall shear stress; OSI, oscillatory shear index.

© Quantitative Imaging in Medicine and Surgery. All rights reserved.

reported that the OSI of the aneurysm enhanced area was lower than that of the nonenhanced area. The results of Lv *et al.* (18) and Khan *et al.* (19) showed that the OSI of aneurysms with AWE was higher than that of aneurysms with no AWE, although without statistical differences. These results are also consistent with ours, which showed that some aneurysms with AWE had a negative correlation between AWE and OSI, and most aneurysms with AWE had a positive correlation between AWE and OSI.

The workflow proposed in this study provided a direct observation of the distribution pattern of AWE from HR-MRI and hemodynamic parameters from 4D-flow MRI. This provided new insights into the inflammation characteristics of the aneurysm wall and its interaction with different hemodynamic conditions from the individual-patient level. It is noteworthy that inflammation is not the only cause of aneurysmal enhancement in HR-MRI images. For example, several studies have found that near-wall slow flow could lead to aneurysmal pseudo-enhancement signals (9-12). Even though the method of sampling signal intensities outside of the aneurysmal wall reduces the impact of pseudo-enhancement, luminal contamination due to errors is inevitable. A more refined approach would help to circumvent this confusion. With more characteristics explored in future studies, such as aneurysm wall thickness or aneurysm tissue section, the mechanism through which hemodynamics interacts with wall inflammation and the mechanism of UIAs rupture may be comprehensively and meticulously elucidated.

Limitation

Although 4D-flow MRI enables qualitative and quantitative *in vivo* analysis of hemodynamics, the trade-off between the scan time and spatial resolution of 4D-flow MRI limits its spatial resolution. Therefore, aneurysms with a diameter <4 mm were not included in this study. This may have reduced the generalizability of our findings. Furthermore, the limited resolution of 4D-flow MRI might underestimate the results of WSS (35). In addition, mapping of signal intensities that indicate AWE may contain luminal pseudo-enhancement caused by low-flow patterns. Finally, comparisons in this study were aneurysm-specific metrics, which did not accommodate comparisons among aneurysms. More human histological evidence is needed to demonstrate the associations between hemodynamics and aneurysm wall inflammation.

Conclusions

The results of this study showed that the spatial distribution of WSS was negatively correlated with AWE in aneurysms with AWE, and OSI was positively correlated with AWE in most aneurysms with AWE from the individual-patient level. However, there might be no correlation between hemodynamics and wall inflammation in aneurysms with no AWE.

Acknowledgments

Funding: This work was supported by the Natural Science Foundation of China (No. 81971604); the Natural Science Foundation of China (No. 81771233); the Natural Science Foundation of Beijing (No. L192013); the Natural Science Foundation of China (No. 81901197); the Natural Science Foundation of Beijing, China (No. 7142032); Beijing Science and Technology Planning Project (No. Z181100009618035); Beijing Municipal Administration of Hospitals' Ascent Plan (No. DFL20190501); Research and Promotion Program of Appropriate Techniques for Intervention of Chinese High-risk Stroke People (No. GN-2020R0007), and Specific Research Projects for Capital Health Development (No. 2018-2-2041). The funders (other than the named authors) had no role in study design, data collection and analysis, decision to publish, or preparation of the manuscript.

Footnote

Reporting Checklist: The authors have completed the STROBE reporting checklist. Available at https://qims.amegroups.com/article/view/10.21037/qims-21-1203/rc

Conflicts of Interest: All authors have completed the ICMJE uniform disclosure form (available at https://qims.amegroups.com/article/view/10.21037/qims-21-1203/coif). AL reports support from the Natural Science Foundation of China (No. 81771233), Beijing Science and Technology Planning Project (No. Z181100009618035), Beijing Municipal Administration of Hospitals' Ascent Plan (No. DFL20190501), and Specific Research Projects for Capital Health Development (No. 2018-2-2041). RL reports support from the Natural Science Foundation of China (No. 81971604), the Natural Science Foundation of Beijing (No. L192013), the Natural Science Foundation of

© Quantitative Imaging in Medicine and Surgery. All rights reserved.

China (No. 81901197), the Natural Science Foundation of Beijing, China (No. 7142032), and Research and Promotion Program of Appropriate Techniques for Intervention of Chinese High-risk Stroke People (No. GN-2020R0007). The other authors have no conflicts of interest to declare.

Ethical Statement: The authors are accountable for all aspects of the work in ensuring that questions related to the accuracy or integrity of any part of the work are appropriately investigated and resolved. The study was conducted in accordance with the Declaration of Helsinki (as revised in 2013). The study was approved by the Institutional Review Board at Tsinghua University and Beijing Tiantan Hospital, and informed consent was provided by all individual participants.

Open Access Statement: This is an Open Access article distributed in accordance with the Creative Commons Attribution-NonCommercial-NoDerivs 4.0 International License (CC BY-NC-ND 4.0), which permits the non-commercial replication and distribution of the article with the strict proviso that no changes or edits are made and the original work is properly cited (including links to both the formal publication through the relevant DOI and the license). See: https://creativecommons.org/licenses/by-nc-nd/4.0/.

References

1. Vlak MH, Algra A, Brandenburg R, Rinkel GJ. Prevalence of unruptured intracranial aneurysms, with emphasis on sex, age, comorbidity, country, and time period: a systematic review and meta-analysis. Lancet Neurol 2011;10:626-36.
2. Li MH, Chen SW, Li YD, Chen YC, Cheng YS, Hu DJ, et al. Prevalence of unruptured cerebral aneurysms in Chinese adults aged 35 to 75 years: a cross-sectional study. Ann Intern Med 2013;159:514-21.
3. Morita A, Kirino T, Hashi K, Aoki N, Fukuhara S, Hashimoto N, Nakayama T, Sakai M, Teramoto A, Tominari S, Yoshimoto T. The natural course of unruptured cerebral aneurysms in a Japanese cohort. N Engl J Med 2012;366:2474-82.
4. Nieuwkamp DJ, Setz LE, Algra A, Linn FH, de Rooij NK, Rinkel GJ. Changes in case fatality of aneurysmal subarachnoid haemorrhage over time, according to age, sex, and region: a meta-analysis. Lancet Neurol 2009;8:635-42.
5. Jufri NF, Mohamedali A, Avolio A, Baker MS. Mechanical stretch: physiological and pathological implications for human vascular endothelial cells. Vasc Cell 2015;7:8.
6. Tulamo R, Frösen J, Hernesniemi J, Niemelä M. Inflammatory changes in the aneurysm wall: a review. J Neurointerv Surg 2018;10:i58-67.
7. Santarosa C, Cord B, Koo A, Bhogal P, Malhotra A, Payabvash S, Minja FJ, Matouk CC. Vessel wall magnetic resonance imaging in intracranial aneurysms: Principles and emerging clinical applications. Interv Neuroradiol 2020;26:135-46.
8. Nagahata S, Nagahata M, Obara M, Kondo R, Minagawa N, Sato S, Sato S, Mouri W, Saito S, Kayama T. Wall Enhancement of the Intracranial Aneurysms Revealed by Magnetic Resonance Vessel Wall Imaging Using Three-Dimensional Turbo Spin-Echo Sequence with Motion-Sensitized Driven-Equilibrium: A Sign of Ruptured Aneurysm? Clin Neuroradiol 2016;26:277-83.
9. Cornelissen BMW, Leemans EL, Slump CH, Marquering HA, Majoie CBLM, van den Berg R. Vessel wall enhancement of intracranial aneurysms: fact or artifact? Neurosurg Focus 2019;47:E18.
10. Gaidzik F, Pravdivtseva M, Larsen N, Jansen O, Hövener JB, Berg P. Luminal enhancement in intracranial aneurysms: fact or feature?-A quantitative multimodal flow analysis. Int J Comput Assist Radiol Surg 2021;16:1999-2008.
11. Cornelissen BMW, Leemans EL, Coolen BF, Peper ES, van den Berg R, Marquering HA, Slump CH, Majoie CBLM. Insufficient slow-flow suppression mimicking aneurysm wall enhancement in magnetic resonance vessel wall imaging: a phantom study. Neurosurg Focus 2019;47:E19.
12. Pravdivtseva MS, Gaidzik F, Berg P, Hoffman C, Rivera-Rivera LA, Medero R, Bodart L, Roldan-Alzate A, Speidel MA, Johnson KM, Wieben O, Jansen O, Hövener JB, Larsen N. Pseudo-Enhancement in Intracranial Aneurysms on Black-Blood MRI: Effects of Flow Rate, Spatial Resolution, and Additional Flow Suppression. J Magn Reson Imaging 2021;54:888-901.
13. Cebral JR, Mut F, Weir J, Putman CM. Association of hemodynamic characteristics and cerebral aneurysm rupture. AJNR Am J Neuroradiol 2011;32:264-70.
14. Chalouhi N, Hoh BL, Hasan D. Review of cerebral aneurysm formation, growth, and rupture. Stroke 2013;44:3613-22.
15. Signorelli F, Sela S, Gesualdo L, Chevrel S, Tollet F, Pailler-Mattei C, Tacconi L, Turjman F, Vacca A, Schul DB. Hemodynamic Stress, Inflammation, and Intracranial Aneurysm Development and Rupture: A Systematic

© Quantitative Imaging in Medicine and Surgery. All rights reserved.

Review. World Neurosurg 2018;115:234-44.
16. Turjman AS, Turjman F, Edelman ER. Role of fluid dynamics and inflammation in intracranial aneurysm formation. Circulation 2014;129:373-82.
17. Xiao W, Qi T, He S, Li Z, Ou S, Zhang G, Liu X, Huang Z, Liang F. Low Wall Shear Stress Is Associated with Local Aneurysm Wall Enhancement on High-Resolution MR Vessel Wall Imaging. AJNR Am J Neuroradiol 2018;39:2082-7.
18. Lv N, Karmonik C, Chen S, Wang X, Fang Y, Huang Q, Liu J. Wall Enhancement, Hemodynamics, and Morphology in Unruptured Intracranial Aneurysms with High Rupture Risk. Transl Stroke Res 2020;11:882-9.
19. Khan MO, Toro Arana V, Rubbert C, Cornelius JF, Fischer I, Bostelmann R, Mijderwijk HJ, Turowski B, Steiger HJ, May R, Petridis AK. Association between aneurysm hemodynamics and wall enhancement on 3D vessel wall MRI. J Neurosurg 2020. [Epub ahead of print].
20. Hadad S, Mut F, Chung BJ, Roa JA, Robertson AM, Hasan DM, Samaniego EA, Cebral JR. Regional Aneurysm Wall Enhancement is Affected by Local Hemodynamics: A 7T MRI Study. AJNR Am J Neuroradiol 2021;42:464-70.
21. Markl M, Frydrychowicz A, Kozerke S, Hope M, Wieben O. 4D flow MRI. J Magn Reson Imaging 2012;36:1015-36.
22. Soulat G, McCarthy P, Markl M. 4D Flow with MRI. Annu Rev Biomed Eng 2020;22:103-26.
23. Zhang M, Peng F, Tong X, Feng X, Li Y, Chen H, Niu H, Zhang B, Song G, Li Y, Liu P, Liu A, Li R. Associations between haemodynamics and wall enhancement of intracranial aneurysm. Stroke Vasc Neurol 2021;6:467-75.
24. Qiao Y, Steinman DA, Qin Q, Etesami M, Schär M, Astor BC, Wasserman BA. Intracranial arterial wall imaging using three-dimensional high isotropic resolution black blood MRI at 3.0 Tesla. J Magn Reson Imaging 2011;34:22-30.
25. Zhang M, Peng F, Li Y, He L, Liu A, Li R. Associations between morphology and hemodynamics of intracranial aneurysms based on 4D flow and black-blood magnetic resonance imaging. Quant Imaging Med Surg 2021;11:597-607.
26. Raghuram A, Varon A, Roa JA, Ishii D, Lu Y, Raghavan ML, Wu C, Magnotta VA, Hasan DM, Koscik TR, Samaniego EA. Semiautomated 3D mapping of aneurysmal wall enhancement with 7T-MRI. Sci Rep 2021;11:18344.
27. Petersson S, Dyverfeldt P, Ebbers T. Assessment of the accuracy of MRI wall shear stress estimation using numerical simulations. J Magn Reson Imaging 2012;36:128-38.
28. Sughimoto K, Shimamura Y, Tezuka C, Tsubota K, Liu H, Okumura K, Masuda Y, Haneishi H. Effects of arterial blood flow on walls of the abdominal aorta: distributions of wall shear stress and oscillatory shear index determined by phase-contrast magnetic resonance imaging. Heart Vessels 2016;31:1168-75.
29. Matouk CC, Cord BJ, Yeung J, Malhotra A, Johnson MH, Minja FJ. High-resolution Vessel Wall Magnetic Resonance Imaging in Intracranial Aneurysms and Brain Arteriovenous Malformations. Top Magn Reson Imaging 2016;25:49-55.
30. Futami K, Kitabayashi T, Sano H, Misaki K, Uchiyama N, Ueda F, Nakada M. Inflow Jet Patterns of Unruptured Cerebral Aneurysms Based on the Flow Velocity in the Parent Artery: Evaluation Using 4D Flow MRI. AJNR Am J Neuroradiol 2016;37:1318-23.
31. Qiu T, Jin G, Xing H, Lu H. Association between hemodynamics, morphology, and rupture risk of intracranial aneurysms: a computational fluid modeling study. Neurol Sci 2017;38:1009-18.
32. Longo M, Granata F, Racchiusa S, Mormina E, Grasso G, Longo GM, Garufi G, Salpietro FM, Alafaci C. Role of Hemodynamic Forces in Unruptured Intracranial Aneurysms: An Overview of a Complex Scenario. World Neurosurg 2017;105:632-42.
33. Takehara Y, Isoda H, Takahashi M, Unno N, Shiiya N, Ushio T, Goshima S, Naganawa S, Alley M, Wakayama T, Nozaki A. Abnormal Flow Dynamics Result in Low Wall Shear Stress and High Oscillatory Shear Index in Abdominal Aortic Dilatation: Initial in vivo Assessment with 4D-flow MRI. Magn Reson Med Sci 2020;19:235-46.
34. Shimizu K, Kataoka H, Imai H, Yamamoto Y, Yamada T, Miyata H, Koseki H, Abekura Y, Oka M, Kushamae M, Ono I, Miyamoto S, Nakamura M, Aoki T. Hemodynamic Force as a Potential Regulator of Inflammation-Mediated Focal Growth of Saccular Aneurysms in a Rat Model. J Neuropathol Exp Neurol 2021;80:79-88.
35. Stalder AF, Russe MF, Frydrychowicz A, Bock J, Hennig J, Markl M. Quantitative 2D and 3D phase contrast MRI: optimized analysis of blood flow and vessel wall parameters. Magn Reson Med 2008;60:1218-31.

Cite this article as: Fu M, Peng F, Zhang M, Chen S, Niu H, He X, Xu B, Liu A, Li R. Aneurysmal wall enhancement and hemodynamics: pixel-level correlation between spatial distribution. Quant Imaging Med Surg 2022;12(7):3692-3704. doi: 10.21037/qims-21-1203

© Quantitative Imaging in Medicine and Surgery. All rights reserved.